Available online at www.sciencedirect.com

SCIENCE DIRECT®

Earth and Planetary Science Letters 235 (2005) 45–61

EPSL

www.elsevier.com/locate/epsl

Radiocarbon simulations for the glacial ocean: The effects of wind stress, Southern Ocean sea ice and Heinrich events

Martin Butzin[a,*], Matthias Prange[b], Gerrit Lohmann[c]

[a]*Department of Geosciences, University of Bremen, P.O. Box 33 04 40, D-28334 Bremen, Germany*
[b]*DFG Research Center Ocean Margins, University of Bremen, P.O. Box 33 04 40, D-28334 Bremen, Germany*
[c]*Alfred Wegener Institute for Polar and Marine Research, P.O. Box 12 0161, D-27515 Bremerhaven, Germany*

Received 5 August 2004; received in revised form 17 February 2005; accepted 1 March 2005
Available online 28 April 2005
Editor: E. Bard

Abstract

Simulations of oceanic radiocarbon for the Last Glacial Maximum are presented, using a three-dimensional global ocean circulation model forced with glacial background states according to various reconstructions. We investigate the influence of sea surface temperatures, sea ice margins, wind stress and Antarctic sea ice formation on the glacial tracer distribution and meridional overturning circulation. The aim of these sensitivity studies is to reconcile available radiocarbon data from marine sediments with reconstructed sea surface temperatures and estimated sea ice production rates. Model runs with a modified freshwater balance in the Southern Ocean, mimicking increased brine release due to enhanced divergence of Antarctic sea ice, arrive at radiocarbon values close to observations. These experiments also yield abyssal temperatures and salinities which are consistent with recent inferences. In the simulation with the best agreement with radiocarbon observations, North Atlantic Deep Water export is reduced by 40% compared to present day, while Antarctic Bottom Water flow is intensified to similar strength in the South Atlantic. Transient simulations show that glacial freshwater discharge into the North Atlantic can cause abrupt increases of atmospheric radiocarbon as observed during Heinrich event 1. However, the effect is only significant in scenarios with a massive short-time discharge at the beginning which is followed by low-level freshwater input for the rest of the event, or if it is assumed that the meridional overturning circulation was already in a modern operational mode.

Keywords: paleoceanography; ocean circulation; radiocarbon; Heinrich events

1. Introduction

What do we know about the large-scale circulation in the Atlantic Ocean at the Last Glacial Maximum (LGM)? Results from coupled general circulation models (GCMs) are contradictory, ranging from

* Corresponding author. Tel.: +49 421 218 82 72; fax: +49 421 218 70 40.
E-mail address: mbutzin@marum.de (M. Butzin).

0012-821X/$ - see front matter © 2005 Elsevier B.V. All rights reserved.
doi:10.1016/j.epsl.2005.03.003

almost vanishing North Atlantic Deep Water (NADW) formation [1] to a significant strengthening of the glacial NADW circulation compared to the present [2]. Paleoceanographers, on the other hand, try to draw information on past circulation modes from marine sediment cores, measuring concentrations of stable carbon, neodymium, oxygen or radioactive isotopes. However, it has been shown that none of these methods allows unambiguous conclusions (cf. [3] and references therein).

A more promising approach is the combined use of data and models. Introducing paleoceanographic proxies into ocean models is not only useful to validate simulations, but also to interpret the data in a reasonable way. So far, only a few studies of the LGM have embarked on this strategy by means of three-dimensional models [4–8]. Previous attempts to simulate the glacial radiocarbon distribution, however, employed surface salinity restoring [4,8], ad hoc freshwater forcing [6] or present-day wind stress [6,7].

Here, we present glacial simulations of radiocarbon (^{14}C) using an ocean general circulation model that avoids these shortcomings. In a series of sensitivity experiments we investigate the influence of various boundary forcing factors on the meridional overturning circulation (MOC) and oceanic ^{14}C distribution, with the aim to reconcile available glacial radiocarbon data from foraminifera and corals with glacial sea surface temperature (SST) reconstructions and estimated rates of sea ice production. We compare the effects of different SST and sea ice fields, and we go further into the question of proper wind stress forcing in such simulations. Special emphasis is placed on the role of the freshwater balance in the Southern Ocean, as recent modeling studies suggest that Antarctic sea ice production and, hence, brine release was substantially enhanced during the LGM, which probably resulted in higher rates of Antarctic Bottom Water (AABW) formation [7,9].

Motivated by abrupt fluctuations in the atmospheric radiocarbon record during Heinrich event 1 [10,11], we finally examine the atmospheric ^{14}C response to ocean ventilation changes caused by massive freshwater discharge into the glacial North Atlantic. These transient simulations provide estimates for atmospheric radiocarbon peaks with respect to different climatic background states, and lead to speculations about the temporal evolution of glacial meltwater input events.

2. Model description and experimental setup

Our model is a modified version of the Hamburg LSG ocean circulation model [12]. It has a horizontal resolution of $3.5^\circ \times 3.5^\circ$ on a semi-staggered 'E'-grid and 22 levels in the vertical direction. For the glacial simulations a global sea level decrease of 120 m is taken into account. The original LSG upstream advection scheme for temperature and salinity has been replaced by a less diffusive third-order QUICK scheme [13] which we applied in this study to radiocarbon as well. Tracer diffusivities are explicitly prescribed. Horizontal diffusivity varies from 10^7 cm^2 s^{-1} at the surface to 5×10^6 cm^2 s^{-1} at the bottom. Vertical diffusivity ranges from 0.3 cm^2 s^{-1} at the surface to 2.6 cm^2 s^{-1} in the deep ocean (which is different to previous work using an 11 level model version [14]).

The ocean is driven by ten-year averaged monthly fields of wind stress, surface air temperature and freshwater flux taken from simulations with the atmosphere general circulation model ECHAM3/T42, which by itself is forced with prescribed values of insolation, CO_2, ice-sheet cover and sea surface temperatures for the present day (PD) as well as for the Last Glacial Maximum. The glacial SST forcing for ECHAM3 comes from two alternative data sets. For one set of experiments we utilize the CLIMAP reconstruction [15] with an additional cooling of 3 °C in the tropics between 30°N and 30°S [16]. For the other set of experiments, the new GLAMAP 2000 reconstruction (see [17] and references therein) is employed in the globally extended version of Paul and Schäfer-Neth [18]. In the Atlantic Ocean the GLAMAP reconstruction is significantly different from that provided by CLIMAP. The GLAMAP SST patterns display higher values in the North Atlantic, but cooling in the tropical and South Atlantic. Correspondingly, the GLAMAP sea ice cover in the North Atlantic is significantly reduced, proposing ice-free Nordic Seas during summer and a winter sea ice margin similar to the CLIMAP sea ice boundary for summer. In the Atlantic sector of the Southern Ocean, GLAMAP finds more sea ice in the Drake Passage

during winter, but less sea ice at the northern boundary of the Weddell Sea.

A scheme for continental runoff closes the hydrological cycle of our ocean model. There is no local flux correction applied; however, freshwater fluxes into the North Atlantic and the Arctic Ocean are reduced by 5% and redistributed over the World Ocean. We apply a surface heat flux formulation based on an atmospheric energy balance model with diffusive lateral heat transports [14] which enables the simulation of observed/reconstructed sea surface temperatures within reasonable error margins (in all equilibrium experiments the global root-mean-square deviation between modeled and observed/reconstructed annual-mean SST is smaller than 1.7 °C). Moreover, this approach permits free adjustment of surface temperatures and salinities due to changes in the ocean circulation, which is crucial in transient experiments as discussed in Section 5 (see also [19]).

Radiocarbon is treated as $\Delta^{14}C$ in the way of Toggweiler et al. [20], with an air–sea gas exchange formulation accounting for glacial climatological boundary conditions. Marine biological processes are neglected because it has been shown that these effects play a minor role for $\Delta^{14}C$ in comparison to the changes induced by circulation and radioactive decay [21,22]. The ocean model is run with fixed boundary conditions for at least 20 000 years into a quasi steady state. It is calibrated in a simulation of anthropogenic radiocarbon which starts from the present-day steady state and considers transient values of atmospheric $\Delta^{14}C$ and CO_2 for the period 1765–1995. Further details about the treatment of radiocarbon in our model can be found in Appendix A.

Radiocarbon data are frequently quoted in the form of ages, via $^{14}C\ \text{age} = t_{1/2} \cdot \ln(^{14}R_a/^{14}R_o)/\ln 2$, where $t_{1/2} = 5730$ years is the true half-life of ^{14}C, and $^{14}R_a$ and $^{14}R_o$ are the $^{14}C/^{12}C$ ratios in atmosphere and ocean, respectively. High radiocarbon concentrations in water translate into low radiocarbon ages and vice versa. Although 'age' is actually not a tracer, we will discuss $\Delta^{14}C$ mostly in terms of (^{14}C) years, because this scale allows a direct comparison between present-day and glacial simulations which employ different atmospheric boundary values of 0‰ and 350‰, respectively. Tracer ages may be biased by nonlinear mixing effects, and for this reason the ^{14}C ages should not be considered as the 'true' water mass age.

3. Present-day ocean control run

Our present-day control experiment PD yields transports of 15 Sv (1 Sv = 1×10^6 m^3/s) of North Atlantic Deep Water in the South Atlantic at 30°S (Fig. 1). NADW formation occurs north of 60°N, with the major convection sites in the North Atlantic located in the Labrador and Nordic Seas. The present-day MOC shows little recirculation in the North Atlantic, which is in contrast to earlier LSG simulations using the more diffusive upstream transport scheme [12].

The modeled distribution of $\Delta^{14}C$ for the present day agrees well with observations [23] from the Atlantic and the Pacific (Fig. 2a–d). Differences in surface and thermocline water may be attributed to the effect of decreasing atmospheric $\Delta^{14}C$ values caused by the combustion of fossil fuels, which is evident in the prebomb observations but not considered in the preindustrial control run. The model results tend to elevated concentrations or younger water mass ^{14}C ages in the deep Southern Ocean. We find natural background $\Delta^{14}C$ values equivalent to radiocarbon ages of about 600 years in upper level and thermocline water. Apparent surface water ages ('surface reservoir ages') are about 400 years (global-mean value of the ice-free areas ≈ 370 years) and increase up to 800 years in the polar regions (Fig. 3a). This is consistent with preindustrial reservoir ages which can be derived from the GLODAP data set [23] or from scattered marine samples published in calibration

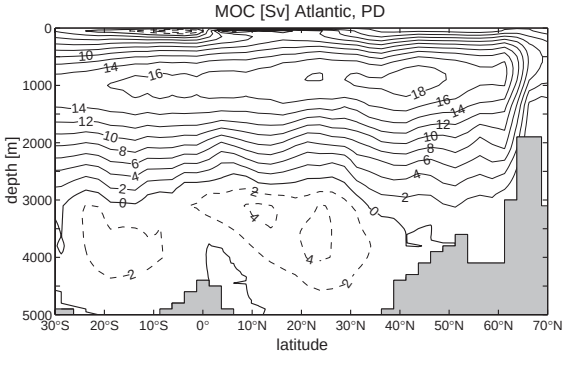

Fig. 1. Meridional overturning circulation (MOC, 1 Sv = 1×10^6 m^3/s) of the Atlantic Ocean, resulting from the present-day (PD) ocean control experiment.

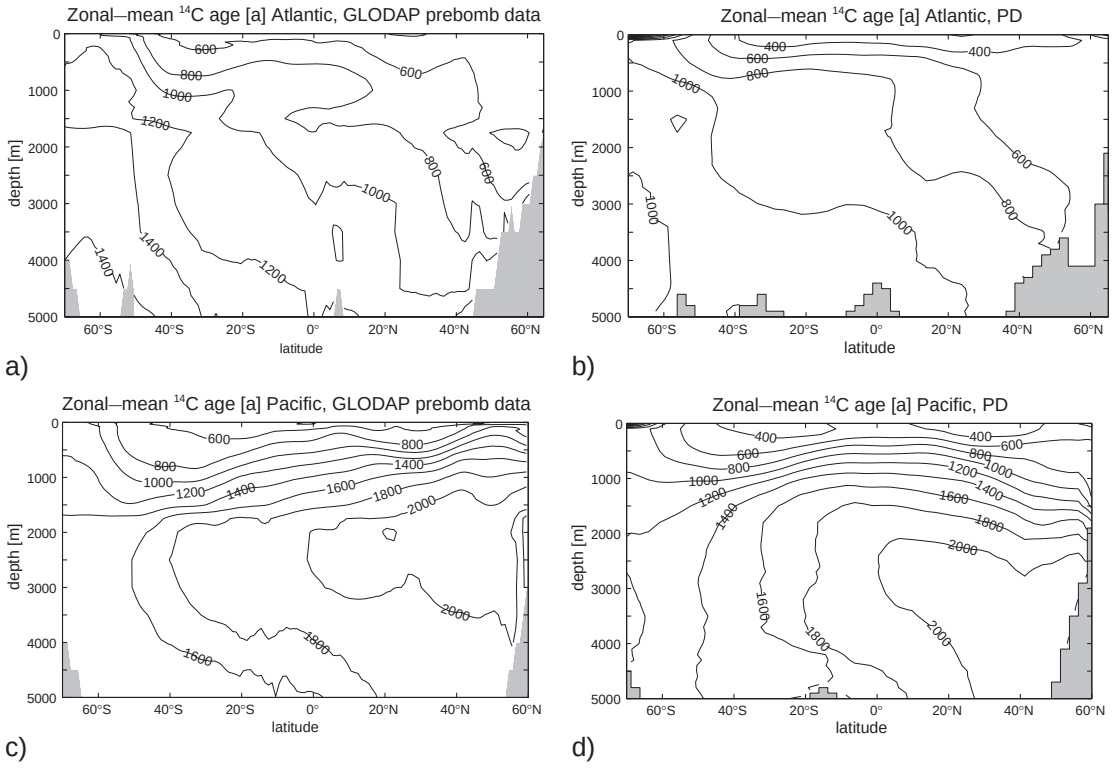

Fig. 2. Zonal-mean radiocarbon ages for the Atlantic and Pacific. a) Prebomb distribution for the Atlantic derived from observations [23], b) preindustrial distribution for the Atlantic resulting from the PD control run, c) prebomb distribution in the Pacific derived from observations [23], d) preindustrial distribution for the Pacific resulting from the PD control run.

studies (e.g., [24]; cf. also the Marine Reservoir Correction Database, http://www.qub.ac.uk/arcpal/marine). Radiocarbon-based apparent age differences between surface water and bottom water ('top-to-bottom age differences') are in the range of 400 to 2000 years. The lowest values are found in the Atlantic while the highest top-to-bottom age differences occur in the North Pacific (Fig. 3b).

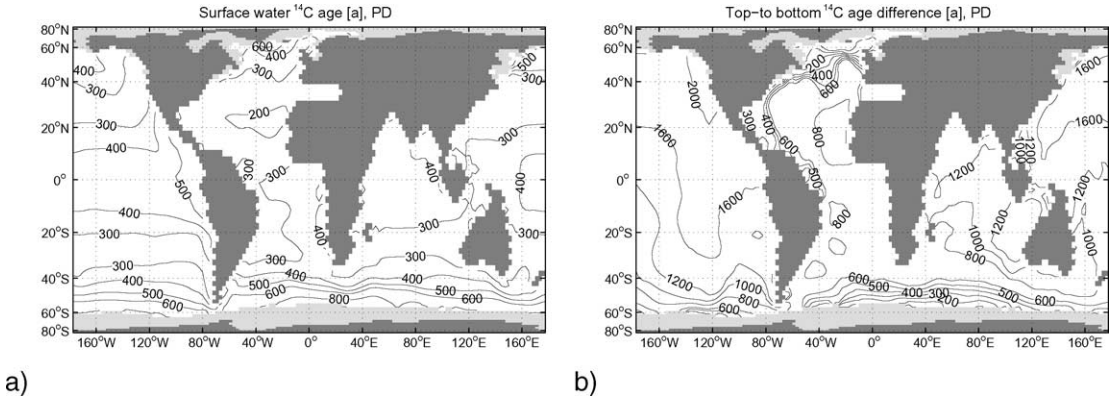

Fig. 3. Horizontal distribution of ^{14}C ages for the preindustrial PD ocean. a) Apparent surface water age (surface reservoir age), b) apparent age difference between bottom water and surface water (top-to-bottom age difference). Light gray areas mark the maximal sea ice extent.

4. Glacial ocean simulations

4.1. Basic ocean simulations and the effects of different SST reconstructions

Table 1 gives an overview of all model experiments discussed in this paper. Experiment CB results in a weak and shallow MOC which is characterized by 5 Sv net export of NADW and 1 Sv transport of AABW in the Atlantic at 30°S (Fig. 4a). In thermocline and intermediate water the $\Delta^{14}C$ values (Fig. 4b) are lower than at present day, equivalent to increasing ^{14}C ages by 100–500 years (cf. Fig. 2b). We find an age increase by up to 800 years for NADW, but a drop by 300 years in North Pacific Deep Water (not shown). In large areas, surface reservoir ages amount to 600 years and increase to more than 1000 years close to the sea ice margins (global-mean value of ice-free areas ≈ 670 years, cf. Fig. 5a). The top-to-bottom age differences increase in the Atlantic by about 200 years while they decrease by roughly the same amount in the Indian Ocean and by 200–400 years in the Pacific, respectively (Fig. 5b).

Using GLAMAP forcing in experiment GB, the Atlantic MOC adjusts to NADW export of 10 Sv, while AABW flow almost vanishes (Fig. 4c). The $\Delta^{14}C$ values in this simulation are elevated relative to experiment CB and appear to be up to 600 years younger than CB in the deep North Atlantic (Fig. 4d), whereas in the other oceans the differences are small. The GB surface reservoir ages are about 50 years lower than in CB (global-mean value of ice-free areas ≈ 620 years, cf. Fig. 5c) but still higher than in the PD ocean. The top-to-bottom age differences in the Atlantic and in the Indian Ocean are the smallest ones of all our experiments. In the Pacific there are no significant changes relative to CB while the GB top-to-bottom age differences decrease by 200–400 years relative to PD (Fig. 5d). The ocean is warmer than in simulation CB. As can be seen in Fig. 6a and b, this is especially true for the upper levels and the North Atlantic. However, in both 'basic' simulations the deep water is generally too warm and to fresh compared to reconstructions (e.g., [40]).

4.2. Influence of surface wind stress

Our glacial forcing fields display considerable differences to the present-day atmosphere (see [25] for a thorough discussion). In general, there is

Table 1
Overview of model experiments and radiocarbon boundary conditions

Experiment	Description	Forcing	Atmospheric $\Delta^{14}C$ (‰)	pCO_2 (μatm)
PD	Present-day control run	Present-day SST	0	280
CB	Basic glacial simulation	CLIMAP SST with 3 °C cooling in the tropics	350	200
GB	Basic glacial simulation	GLAMAP SST	350	200
CW	Glacial simulation with present-day winds	CLIMAP SST with 3 °C cooling in the tropics, present-day winds	350	200
GW	Glacial simulation with present-day winds	GLAMAP SST, present-day winds	350	200
CS	Glacial simulation with a modified freshwater balance in the Southern Ocean	CLIMAP SST with 3 °C cooling in the tropics, add. brine release in the Southern Ocean	350	200
GS	Glacial simulation with a modified freshwater balance in the Southern Ocean	GLAMAP SST, add. brine release in the Southern Ocean	350	200
HPD	Transient simulation of a Heinrich event	Present-day SST, variable freshwater discharge into the North Atlantic	variable, initial value=0	280
HGS	Transient simulation of a Heinrich event	GLAMAP SST, add. brine release in the Southern Ocean, variable freshwater discharge into the North Atlantic	variable, initial value=350	200

higher glacial wind stress, especially at mid and high latitudes (Fig. 7). CB winds have a more zonal structure than present-day winds. Case GB with ice-free Nordic seas yields, for the North Atlantic, southwesterly winds similar to PD conditions. In order to investigate the effect of glacial winds on ocean dynamics and air–sea gas exchange (which depends on the wind speed according to Eq. (A4) in Appendix A), we perform two sensitivity experiments, CW and GW, in which the original CB and GB winds are replaced by PD winds. In both cases, the meridional overturning circulation in the Atlantic is hardly affected, but ^{14}C ages increase by up to 200 years in the deep and abyssal North Atlantic (Fig. 8). Conversely, we find radiocarbon ages decreasing by roughly the same amount in parts of the Pacific Deep Water layer (not shown). These changes propagate into increasing top-to-bottom radiocarbon age differences of up to 300 years in the North Atlantic, while in parts of the North Pacific the top-to-bottom ^{14}C age differences drop by 100–200 years (not shown).

Experiments CW and GW demonstrate that fully glacial climatological boundary conditions are necessary for realistic simulations of oceanic radiocarbon at the LGM, and that glacial winds cause intensified ventilation of the deep ocean with radiocarbon. However, we note that the wind effect can be counterbalanced by other factors such as lower atmospheric CO_2 concentrations, as indicated by the generally elevated glacial surface reservoir ages, or such as increased sea ice cover (which was shown by [4,7]).

4.3. Effects of a modified freshwater balance of the glacial Southern Ocean

Since sea ice dynamics is not explicitly included in our model setup, we carry out additional experiments (named CS and GS) with a modified fresh-

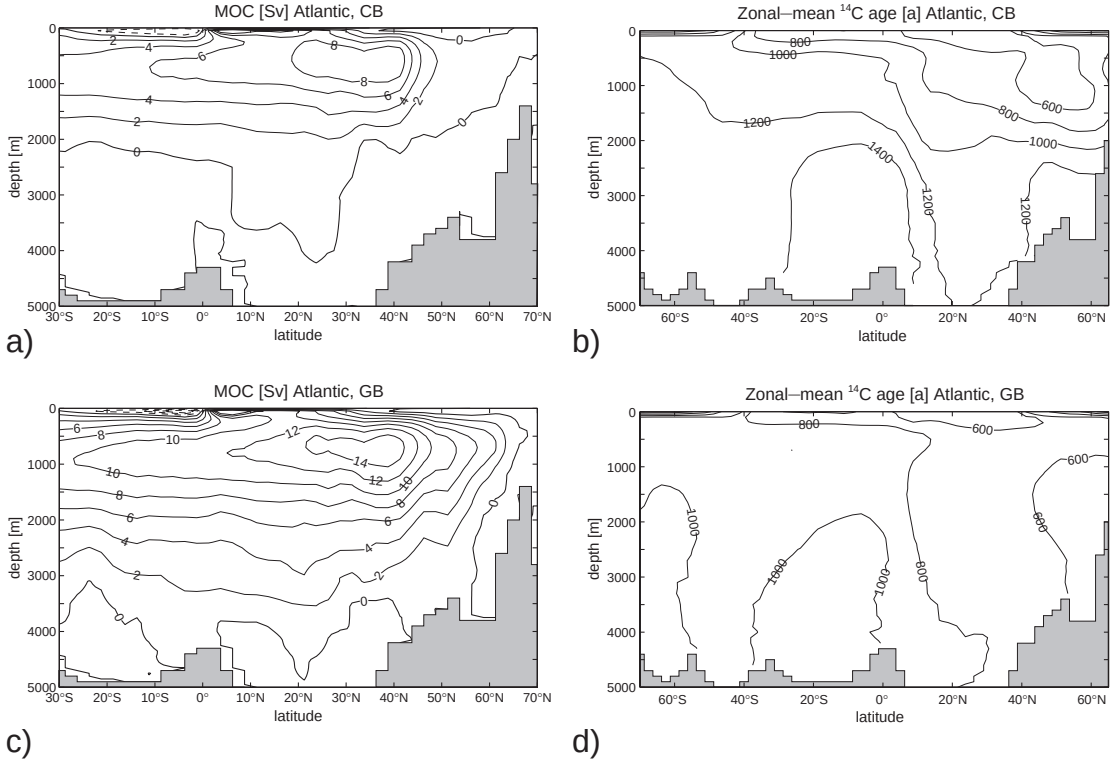

Fig. 4. Meridional overturning and radiocarbon of the LGM ocean, shown are results for the Atlantic. a) Meridional overturning circulation for CB, b) zonal-mean water mass ^{14}C age for CB, c) MOC for GB and d) zonal-mean water mass ^{14}C age for GB.

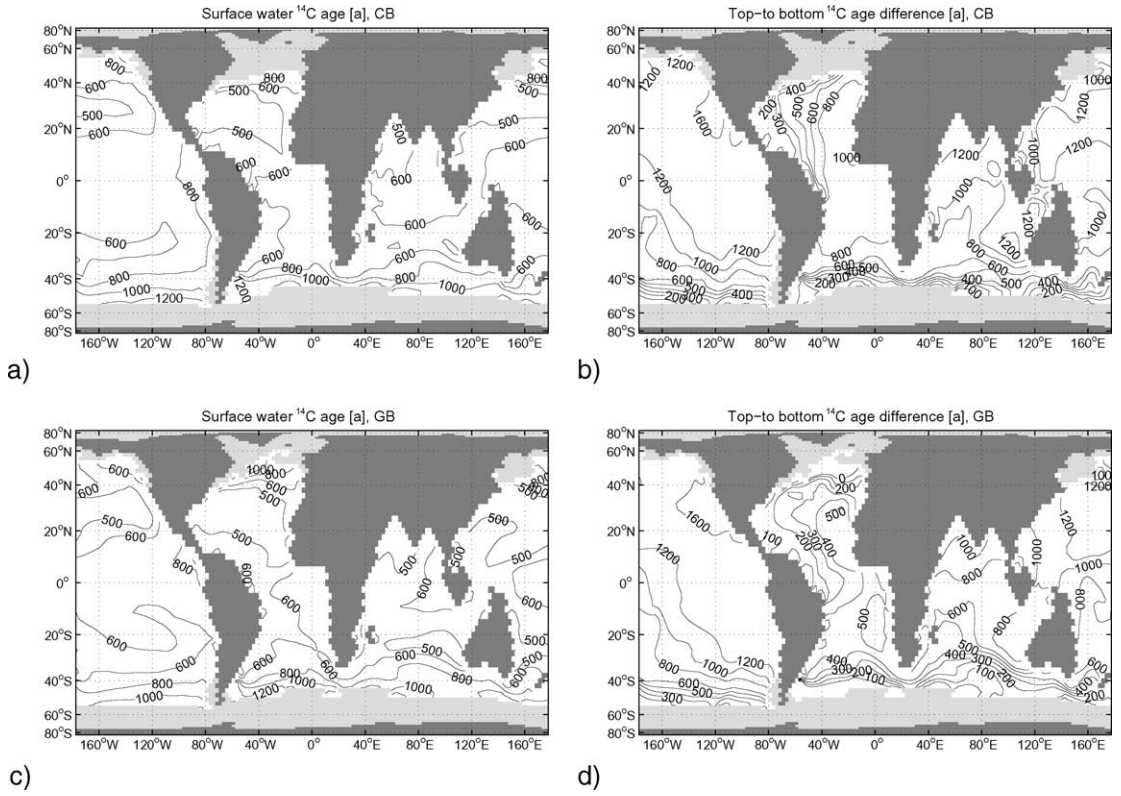

Fig. 5. Horizontal distribution of ^{14}C ages for the LGM ocean. a) surface reservoir age for simulation CB, b) top-to-bottom age difference for CB, c) surface reservoir age for experiment GB and d) top-to-bottom age difference for GB. Light gray areas mark the maximal sea ice extent.

water balance of the Southern Ocean, mimicking an enhanced northward sea ice export as suggested by recent LGM modeling studies [7,9]. Based on the simulations by Shin et al. [9] we account for a zonally homogeneous haline density flux change of about 1.8×10^{-6} kg m^{-2} s^{-1} (equivalent to a total freshwater export of approximately 1.9 Sv) from the sea ice production zone south of 60°S to the region with enhanced summer sea ice melting at the LGM (50–55°S).

In experiment CS, NADW flow in the Atlantic shoals to intermediate depths and amounts to 3 Sv at 30°S, while the AABW layer thickens with 5 Sv northward export at the same latitude (Fig. 9a). Compared to the basic simulations, changes of $\Delta^{14}C$ in the surface water layer are small (Fig. 9b), and the global-mean surface water reservoir age of about 630 years in the ice-free areas is close to the value of CB (Fig. 10a). Deep and bottom water in the Atlantic is considerably depleted with radiocarbon (Fig. 9b). Compared to simulation CB, we find decreased radiocarbon concentrations in the abyssal North Pacific and elevated $\Delta^{14}C$ values in the eastern South Pacific (not shown). Correspondingly, the CS top-to-bottom ^{14}C age differences increase throughout in the Atlantic and in the North Pacific (Fig. 10b).

In simulation GS, the water mass transports in the South Atlantic at 30°S amount to 7 Sv for NADW and 5 Sv for AABW, respectively (Fig. 9c). The distribution of $\Delta^{14}C$ in the upper level Atlantic bears similarities with the pattern of experiment CB, but with an negative offset corresponding to about 200 years (cf. Figs. 2b and 9d, respectively). When compared with simulation GB, radiocarbon ages increase by up to 700 years in NADW and by 200–400 years in the deep and abyssal North Pacific, respectively, while the entire South Pacific (shown in Fig. 9e) appears to be younger by up to 400 years. Again, ^{14}C changes in surface water are small. In

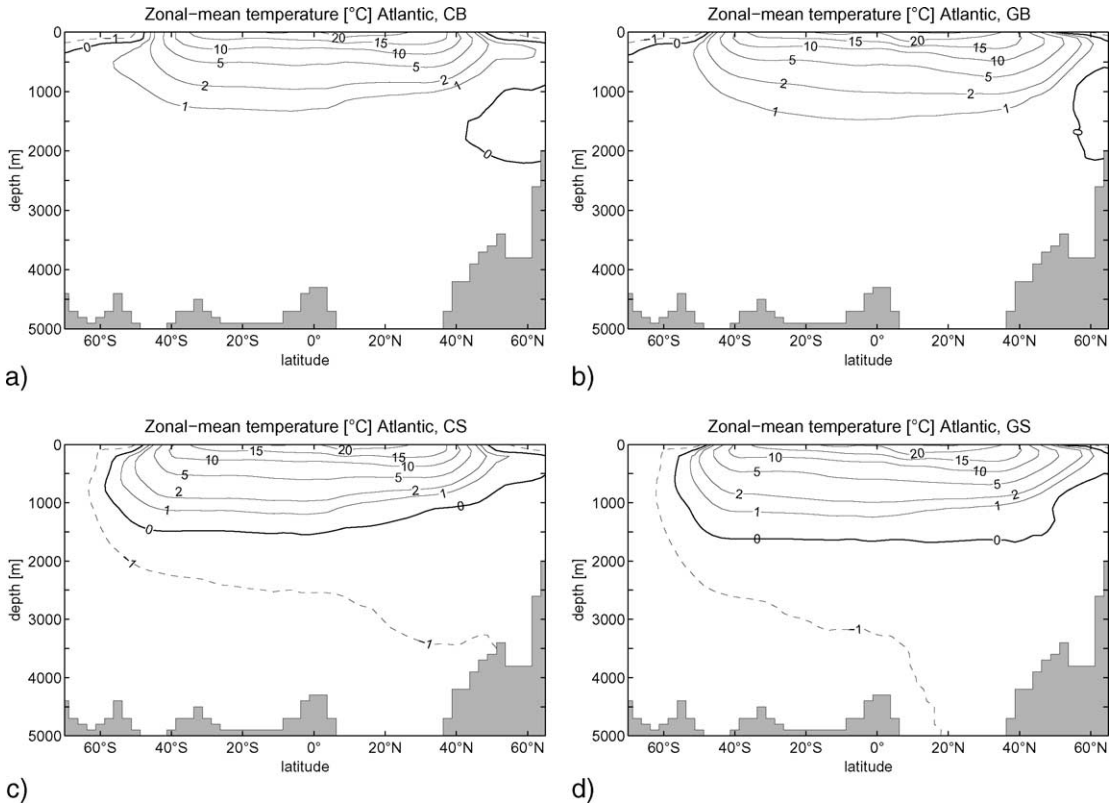

Fig. 6. Zonal-mean potential temperature in the Atlantic Ocean resulting from various LGM simulations. a) CB, b) GB, c) CS and d) GS. Figures c) and d) refer to experiments with a modified freshwater balance in the Southern Ocean, see Section 4.3 for a further explanation.

terms of the surface water reservoir age, the global-mean value of the ice-free areas amounts to about 590 years (Fig. 10c). Compared to GB, the top-to-bottom ^{14}C age differences increase by 200–800 years in the Atlantic while they drop by roughly the same amount in the South East Pacific (cf. Figs. 5d and 10d).

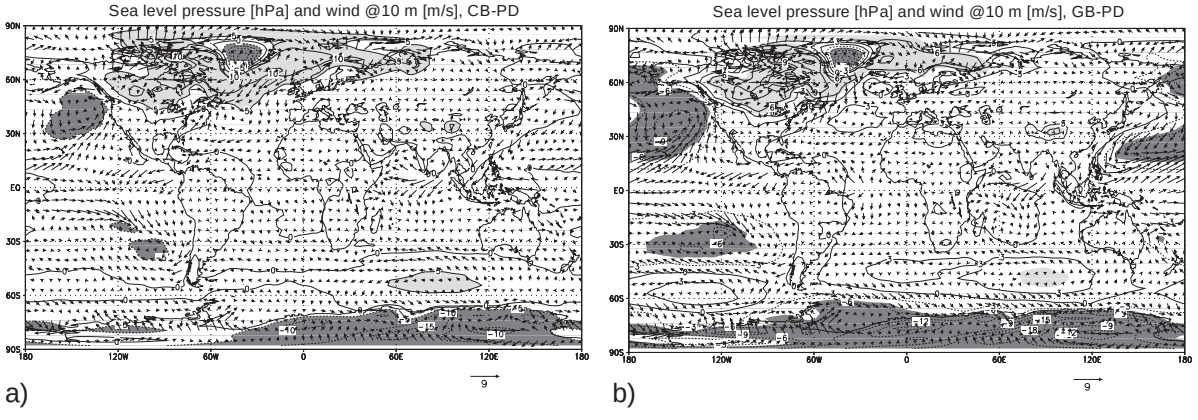

Fig. 7. Anomalies of sea-level pressure and surface wind velocity between the Last Glacial Maximum and present-day conditions. a) CB-PD, b) GB-PD.

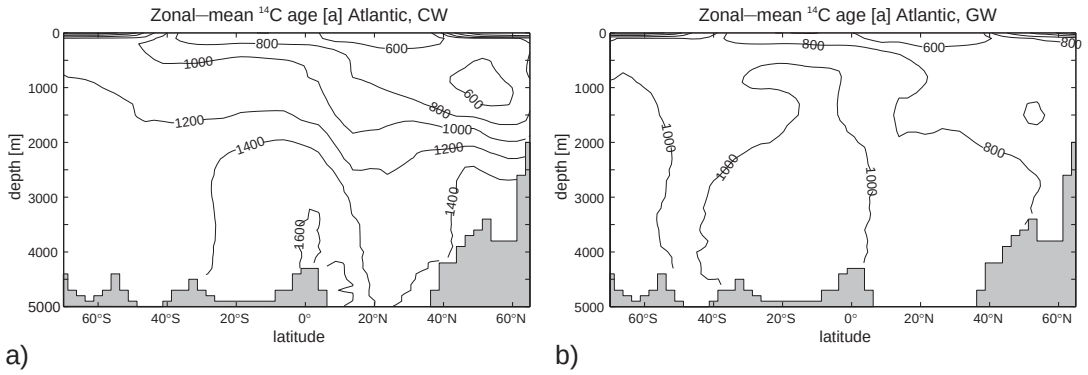

Fig. 8. Zonal-mean water mass radiocarbon ages according to simulations of the glacial ocean forced with PD wind fields, shown are results for the Atlantic. a) for CW, b) for GW.

Fig. 11 shows a compilation of radiocarbon ages for the glacial ocean on the basis of marine sediment and coral data [26–34,36,37,39]. The apparent top-to-bottom age differences range from less than 100 years up to 5000 years, with the restrictions that some values do not refer to the LGM period, and that to some extent there is also considerable data scatter. The latter is especially the case in the Pacific where, in the eastern equatorial region, this may be due to contamination problems [38,39]. Experiments GS and, to a lesser extent, CS lead to top-to-bottom ^{14}C age differences which are consistent with the observations. The 'basic' glacial ocean simulations CB and GB, however, have difficulties reproducing the global pattern of observed ^{14}C age differences. Experiments GS and CS are also remarkable in that they arrive at abyssal temperatures below -1 °C (shown in Fig. 6c and d) and salinities of about 36.5 (not shown) close to recent reconstructions [40].

Ventilation intensity and structure of the glacial overturning circulation are still subject of discussion. In this issue, top-to-bottom ^{14}C age differences are often interpreted as a measure of ventilation intensity (e.g., [29]), although the relationship between tracer data (whether concentrations or ages) and mass fluxes is generally not straightforward. Here, we refer to top-to-bottom age differences for comparison with observations only and infer glacial ventilation intensities from the simulated velocity fields. The best agreement with ^{14}C observations is achieved by simulation GS. This experiment indicates an NADW overturning cell which is shallower and weaker by about 40% compared to the present. As to the AABW layer, simulation GS reveals a flow regime which is of equal strength in the South Atlantic. A slowdown of the glacial 'conveyor belt' is consistent with the reasoning of Broecker [35,39].

5. Impact of Heinrich event-like freshwater pulses into the North Atlantic

Geological records from the last glacial period show anomalous occurrences of ice-rafted debris in the North Atlantic (Heinrich events) which are associated with shutdowns of the MOC and global-scale climatic changes (e.g., [41]). The Oldest Dryas cooling around Heinrich event H1 at about 17.5 kyr BP is marked by a rapid increase of atmospheric Δ^{14}C by about 50–100‰ [10,11]. Here, we investigate the potential effect of Heinrich events on the late-glacial radiocarbon record with two series of transient simulations in which we apply freshwater perturbations to the Atlantic MOC. Series HPD is initialised with the present-day configuration and serves for control purposes, while series HGS starts from the equilibrium simulation GS. During the transient simulations the ocean is coupled with an instantaneously mixed atmospheric ^{14}C reservoir which in turn is connected with a simple model of the terrestrial biosphere (see Appendix A for a further description). From a spinup integration of the steady state radiocarbon system we diagnose a (cosmogenic) production rate of atmospheric ^{14}C necessary to balance air–sea exchange and radioactive decay. The diagnosed radiocarbon production fluxes amount to 1.73 atoms cm^{-2} s^{-1} for present-day and 2.56 atoms cm^{-2} s^{-1}

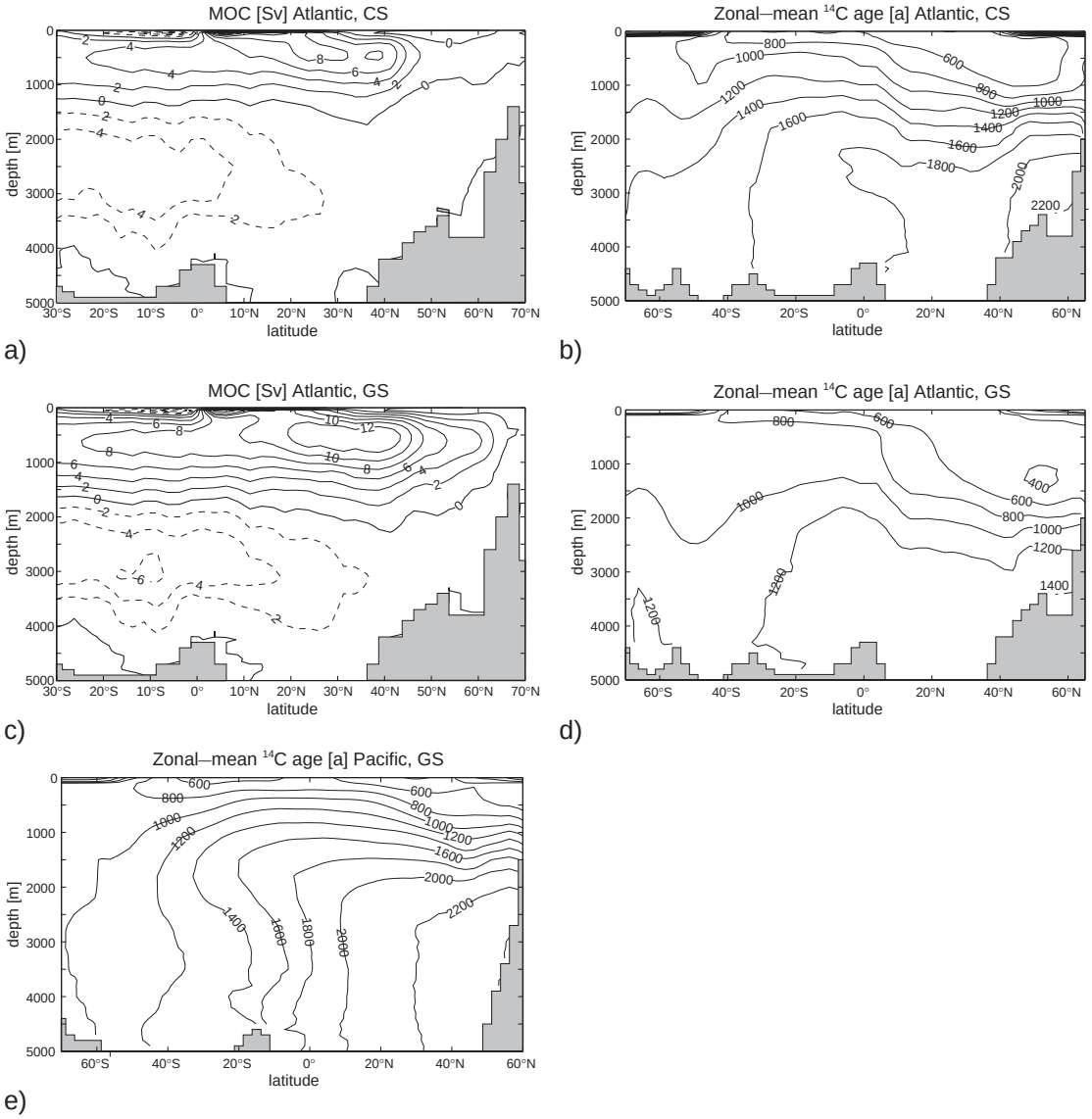

Fig. 9. Meridional overturning circulation and radiocarbon according to simulations of the glacial ocean with a modified freshwater balance in the Southern Ocean. a) Atlantic MOC for CS, b) zonal-mean water mass ^{14}C age in the Atlantic for CS, c) Atlantic MOC for GS, d) zonal-mean water mass ^{14}C age in the Atlantic for GS and e) zonal-mean water mass ^{14}C age in the Pacific for GS.

for glacial conditions, respectively. These numbers are close to cosmogenic production estimates for the Holocene (2.02 atoms cm^{-2} s^{-1} [42]) and for the LGM (about 30% higher than the present ^{14}C production [43]). We then inject freshwater into the North Atlantic between 40° and 55° N, choosing square-shaped discharge curves with amplitudes of 0.3 Sv, 0.5 Sv, 1.0 Sv and 1.5 Sv, with corresponding input periods of 500, 300, 150 and 100 years, respectively. The freshwater input totals 4.7×10^{15} m^3 which is equivalent to a global sea level rise of 13 m. The input scenario with the smallest amplitude corresponds to recent discharge estimates [41], while the other experiments serve to explore the response of the ocean–atmosphere radiocarbon system to peak values of freshwater discharge. Since we are inter-

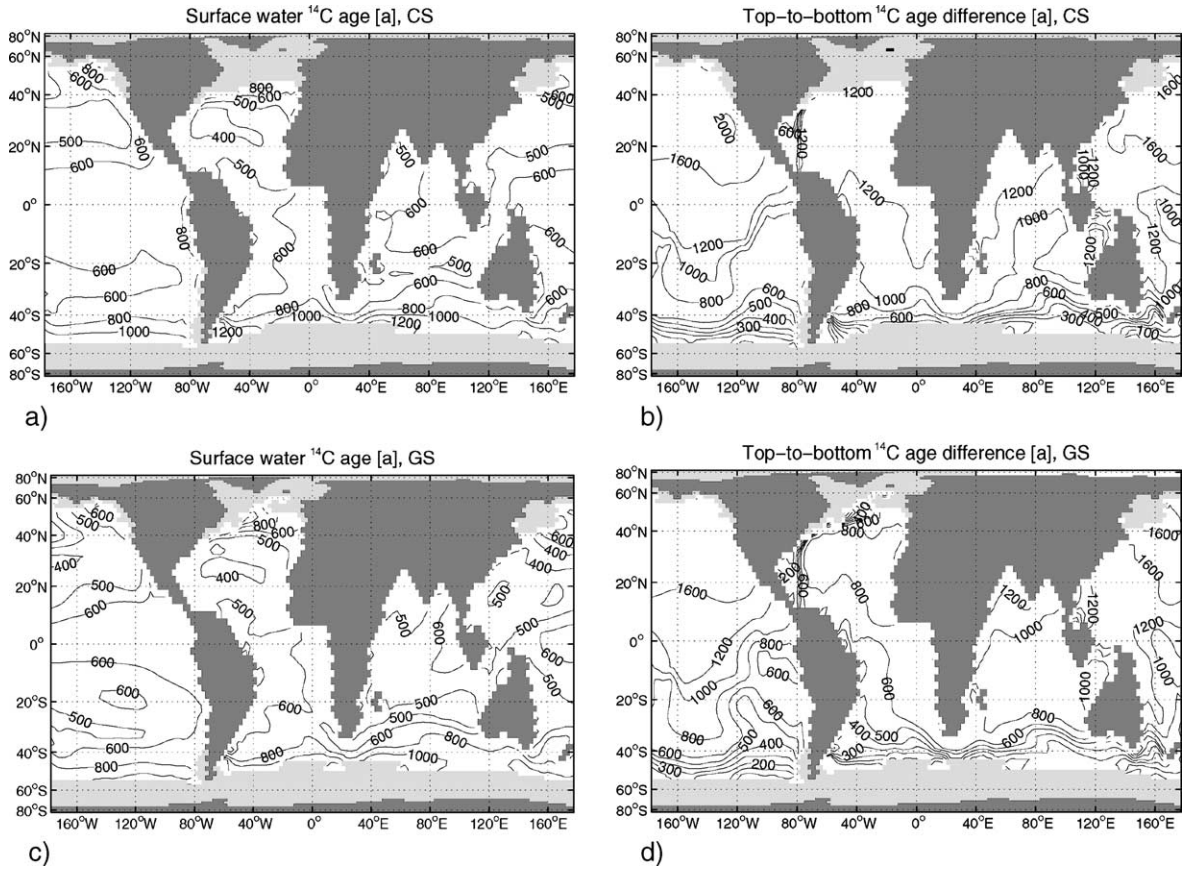

Fig. 10. Horizontal distributions of ^{14}C ages according to simulations of the LGM ocean with a modified freshwater balance in the Southern Ocean. a) Surface reservoir age for simulation CS, b) top-to-bottom age difference for CS, c) surface reservoir age for experiment GS and d) top-to-bottom age difference for GS. Light gray areas mark the maximal sea ice extent.

ested in separating the impact of ocean ventilation changes, we do not consider variations of cosmogenic ^{14}C production.

In all experiments the freshwater injection causes a considerable weakening of the Atlantic MOC, and in some cases NADW formation almost ceases (see Figs. 12a and 13a). As a consequence, the deep sea is less effectively ventilated and the radiocarbon water mass ages increase in all ocean basins below 1000 m depth. The largest ventilation changes occur in the far North Atlantic, while the deep Pacific Ocean is less affected. These changes imply that top-to-bottom ^{14}C age differences temporarily increase by more than 1000 years in the North Atlantic and by about 100–500 years in other regions of the world ocean. Our simulations do not show increasing surface reservoir ^{14}C ages that have been reported for freshwater discharge events [44]. We suppose that these are regional-scale effects due to convection events or changes in sea ice transport which are not captured by our model. After the end of the freshwater perturbation the overturning circulation recovers and the deep-sea ventilation restarts.

More precisely, in series HPD the ^{14}C ages of NADW increase with the duration of the freshwater input by 500 to 1000 years. Deep and bottom waters in the North Pacific show ^{14}C age increases of about 200 years independent of the duration of meltwater discharge. After the end of the freshwater perturbation the Atlantic MOC fully recovers within thousand years (Fig. 12a). However, during the first 500 years of the recovery process the deep ocean ventilation remains weak, which leads to further water mass aging in the deep sea. All HPD experiments eventually arrive at

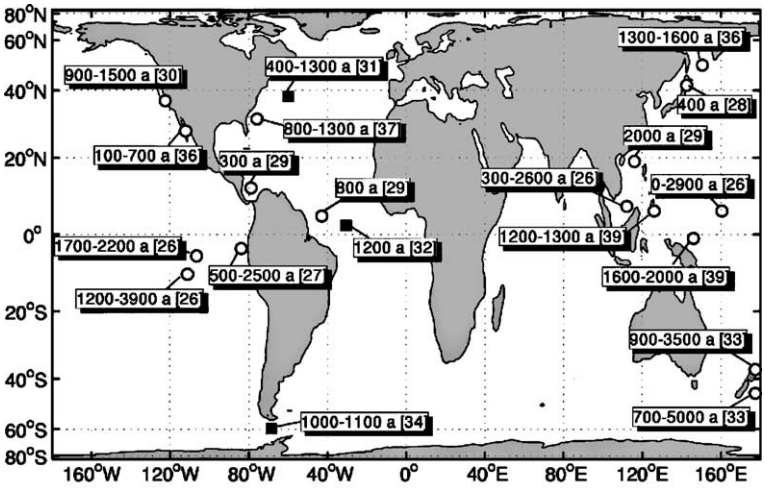

Fig. 11. Map of top-to-bottom ^{14}C age differences (rounded to ± 100 years) for the glacial ocean, based on foraminifera (open circles) and deep-sea corals (filled squares). Differences to original values are due to age corrections for changing atmospheric ^{14}C applied by [34,35].

similar maximum water mass ages, of about 1700 years in the deep/abyssal North Atlantic and about 2500 years in the North Pacific, respectively.

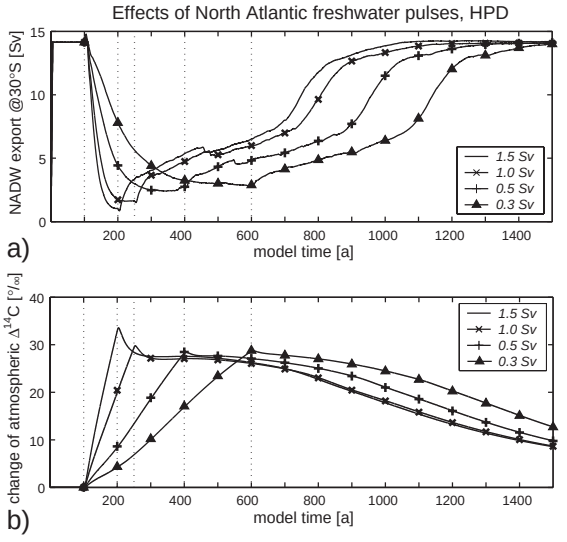

Fig. 12. Simulated effects of freshwater perturbations in the North Atlantic realm, present-day background conditions (HPD). Shown are results for a total freshwater input of 4.7×10^{15} m^3 (equivalent to a global sea level rise of about 13 m), which is injected with different discharge rates. a) NADW export in the South Atlantic at 30°S (in Sv), b) change of atmospheric $\Delta^{14}C$ (in ‰). Dotted lines mark beginning and end of the freshwater input.

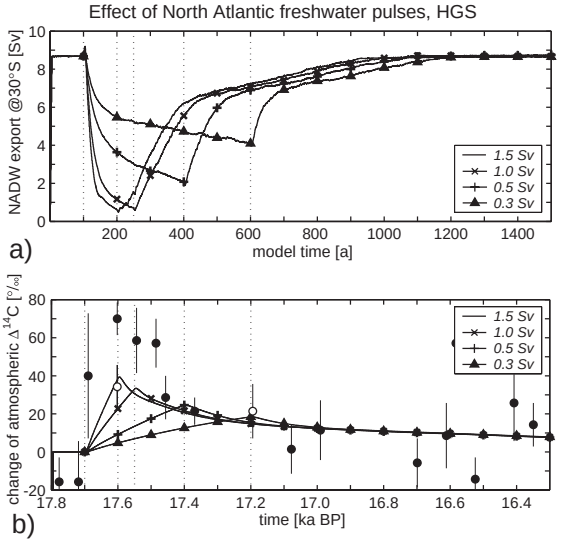

Fig. 13. Simulated effects of freshwater perturbations in the North Atlantic realm, glacial background conditions (HGS). Shown are results for a total freshwater input of 4.7×10^{15} m^3 (equivalent to a global sea level rise of about 13 m) which is injected with different discharge rates. a) NADW export in the South Atlantic at 30°S, b) change of atmospheric $\Delta^{14}C$, together with detrended observations during the Oldest Dryas around Heinrich event 1 according to [10] (open circles) and [11] (filled circles); the data are redrawn from [56]. Note that the ordinate scaling is different to Fig. 12b. Dotted lines mark beginning and end of the freshwater input.

Simulations HGS lead to age increases by about 200 to 300 years for deep and bottom water in the North Atlantic and North Pacific. The glacial MOC recovers faster than in the present-day control experiments (Fig. 13a), and the deep sea is not only reventilated via the North Atlantic but also from the Southern Ocean. For these reasons there is only a short time lag (if at all) between the end of the freshwater pulse and the peak of deep-water aging. The maximum deep and bottom water ^{14}C ages in the North Atlantic and North Pacific are similar to HPD.

As the ^{14}C concentrations in the deep sea decrease during the freshwater input, radiocarbon accumulates in the upper ocean and in the atmosphere (Figs. 12b and 13b). The atmospheric radiocarbon excursions are correlated with the intensity and the rate of NADW weakening. In the present-day experiments, NADW formation weakens by about 80% with small variations, but the minimum transport values are approached with different time constants (Fig. 12a). Stronger freshwater discharge causes faster deep-sea ventilation cutoff and steeper increase of atmospheric radiocarbon, but eventually the $\Delta^{14}C$ amplitudes arrive at roughly the same values of 29–34‰ (Fig. 12b). This is higher than obtained with an earlier version of the LSG model which, amongst other things, used different schemes for advection and uptake of tracers [45].

The glacial simulations HGS yield atmospheric $\Delta^{14}C$ peak values of 19–40‰ (Fig. 13b). Freshwater input rates of 1.0 Sv and 1.5 Sv lead to somewhat higher atmospheric $\Delta^{14}C$ amplitudes than in HPD, because in these cases the glacial NADW formation is almost stalled. Smaller discharge rates lead to smaller atmospheric $\Delta^{14}C$ amplitudes, because in these scenarios the glacial NADW formation and hence the physical radiocarbon pump to the deep sea are less affected. Our reference scenario with a discharge rate of 0.3 Sv suggests only a modest contribution of ocean ventilation changes to the late-glacial record of atmospheric $\Delta^{14}C$, which is in contradiction to box model results [46]. However, the oceanic impact on atmospheric $\Delta^{14}C$ during Hl would significantly rise in two cases: (1) if we assume a meltwater scenario beginning with massive short-time discharge (e.g., with a rate of more than 1 Sv for a period of about 100 years) which then continues at a much lower or almost vanishing level, or (2) if the ocean actually was already in a modern (say PD) instead of a glacial (GS) operational mode, which would strengthen some previous results obtained with simplified models and using present-day boundary conditions (e.g. [47]).

There are other mechanisms that have been proposed to overcome a similar problem for the Younger Dryas cold interval (about 13 kyr ago). Marchal et al. [48] suggested variations of the cosmogenic radiocarbon production as a driver, while Delaygue et al. proposed a mechanism in which calming of tropical winds leads to decreased vertical exchange in the low-latitude ocean and hence to reduced uptake of atmospheric ^{14}C [49]. We do not think that these mechanisms hold for Hl, because ^{10}Be data from the Greenland Summit ice cores [43] do not indicate significant cosmogenic production changes of ^{14}C for this period, and because our forcing fields are generally characterized by enhanced wind stress for colder conditions (Fig. 7). However, final clarity about the second feedback can only be achieved with fully coupled simulations including a dynamical atmosphere.

6. Conclusions

The state of the glacial large-scale ocean circulation is still an open and controversial issue. A promising approach to tackle this problem is the combination of data and models. In this study, we employed two glacial SST reconstructions (CLIMAP, with an additional cooling of 3 °C in tropics, and GLAMAP) for simulations of $\Delta^{14}C$ and discussed some implications arising.

In general, our simulations reveal a crucial influence of the background climate conditions on the results. It turns out that the oceanic uptake of ^{14}C is rather sensitive to the surface wind speed, and that inadequate wind fields can lead to spurious radiocarbon distributions in the ocean's interior. This calls for a sufficient knowledge of the state of the glacial atmosphere. As an indirect implication it follows that there may be systematic uncertainties introduced by the assumption of climatic steady state conditions during the model spinup. While this is a general problem in climate modeling, it is particularly critical for oceanic radiocarbon due to the long integration time scale of more than 10^4 years. Similar complica-

tions may result from the fact that atmospheric ^{14}C was not constant prior to the LGM (e.g., [50]). Future modeling studies should address these initial value problems by running transient ^{14}C simulations over several 10 000 years.

Furthermore, our model experiments indicate a strong influence of Antarctic sea ice formation on the glacial ocean circulation, and hence on oceanic $\Delta^{14}C$ and other hydrographic parameters. Our basic simulations with fixed sea ice distributions arrive at abyssal radiocarbon concentrations and water temperatures which are too high compared to reconstructions. However, when we assume additional brine release in the Southern Ocean due to enhanced northward export of Antarctic sea ice, AABW formation increases while NADW flow weakens, and the agreement with observations improves substantially. These findings support previous results suggesting that sea ice formation in the Southern Ocean had a crucial effect on the glacial thermohaline circulation [9].

The best agreement with proxy data results from a model configuration using GLAMAP boundary conditions combined with subantarctic brine release. In this case, the deep sea is very cold, saline and depleted in radiocarbon. The latter pretends a sluggish overturning circulation. However, while NADW transport is indeed reduced (by about 40%) and occurs at intermediate depths, it turns out that the abyssal water mass properties are the consequence of actually enhanced AABW flow, matching the weakened NADW export in the South Atlantic.

Finally, our transient experiments partly strengthen previous findings with simplified models that freshwater perturbations of the NADW formation could have induced significant rises of $\Delta^{14}C$ in the glacial atmosphere. The atmospheric radiocarbon amplitude depends on the climatic background state, which sets the efficiency of the physical ^{14}C pump to the deep sea. On the average, simulations under present-day climate conditions yield higher atmospheric $\Delta^{14}C$ peaks than those for LGM climate. Our experiments with different climatic background states are a first step towards simulating the entire $\Delta^{14}C$ record of the last deglaciation, a period that was interspersed with intervals of cooling and warming. Moreover, our results point to the temporal evolution of glacial freshwater discharge events. For a given total discharge of 4.7×10^{15} m^3 according to recent estimates [41], the effect of glacial ocean ventilation changes on atmospheric $\Delta^{14}C$ is only significant if the freshwater input starts with a massive peak discharge, followed then by low-level input during the rest of the period. It will be interesting to see if these proposed findings can be corroborated by other geologic evidence and further simulations.

Acknowledgments

Thanks are due to Stephan Lorenz for performing parts of the ECHAM3 runs, to Andreas Manschke and Silke Schubert for technical assistance, to Robert Key for informations regarding the GLODAP radiocarbon data set, and to Michael Schulz and André Paul for stimulating discussions. Three reviewers made constructive comments that helped to improve the manuscript. This work was funded by the German Bundesministerium für Bildung und Forschung through research programs KIHZ (M.B.) and DEKLIM (G.L.), and by the Deutsche Forschungsgemeinschaft through the Research Center 'Ocean Margins' (M.P.) (No. RCOM0282).

Appendix A

A.1. Atmospheric boundary values and air–sea exchange of ^{14}C

Instead of computing absolute radiocarbon concentrations the LSG model simulates the $^{14}C/^{12}C$ ratio which, to a first approximation, can be considered as a radioconservative tracer [21]. Following Toggweiler et al. [20] the results are scaled to the atmospheric $^{14}C/^{12}C$ ratio during the simulations and converted to $\Delta^{14}C$. The oceanic uptake of radiocarbon is calculated from the air–sea flux F_{ao},

$$F_{ao} = \mu h_{ml}({}^{14}R_a - {}^{14}R_o)(1 - i_f), \quad \text{(A1)}$$

where μ is the exchange rate of $^{14}CO_2$, h_{ml} is the surface layer depth in our model, $^{14}R_a$ and $^{14}R_o$ are the $^{14}C/^{12}C$ ratios in air and surface water, respectively, and i_f is the fractional sea ice cover. In the present-day control experiment, we set $^{14}R_a = 1$ (as the standard $^{14}C/^{12}C$ ratio of 1.176×10^{-12} cancels out during

the conversion to $\Delta^{14}C$), which is equivalent to $\Delta^{14}C = 0‰$. In the calibration simulation of anthropogenic radiocarbon, $^{14}R_a$, varies according to the history of atmospheric $\Delta^{14}C$ for 1765–1990 [51]. For the glacial simulations we assume $^{14}R_a = 1.35$, equivalent to an atmospheric $\Delta^{14}C$ background value of 350‰ (cf. [43,46] and references therein). Additional experiments with different glacial background values (of 0‰ and 300‰, not shown) revealed that, to a first approximation, the actual value of $^{14}R_a$ has a minor influence on the results as long as equilibrium situations and relative quantities (such as radiocarbon ages) are considered. The $^{14}CO_2$ exchange rate is given by

$$\mu = j \Big/ \left(\sum CO_2^* \cdot h_{ml} \right), \quad \text{(A2)}$$

where j is the invasion rate of ^{14}C and $\sum CO_2^* = 2.0$ mol/m^3 is the concentration of total inorganic carbon in surface water. The invasion rate is expressed as:

$$j = \langle k \rangle \alpha p CO_2, \quad \text{(A3)}$$

where $\langle k \rangle$ is the gas transfer velocity, α the solubility of CO_2 in seawater [52] and pCO_2 the atmospheric partial pressure of CO_2. We assume a variable gas transfer velocity as set up by Wanninkhof [53] on the basis of radiocarbon field data:

$$\langle k \rangle = 2.78 \times 10^{-6} \left[0.39 \langle u_{10} \rangle^2 (Sc/660)^{-1/2} \right]. \quad \text{(A4)}$$

Here, $\langle u_{10} \rangle$ is the monthly averaged wind speed at 10 m, and Sc is the Schmidt number (the ratio between the kinematic viscosity of water and the diffusion coefficient of CO_2 in sea water). The atmospheric partial pressure of CO_2 during our glacial experiments is 200 µatm. The PD control experiment is carried out with $pCO_2 = 280$ µatm, while in the calibration simulation of bomb radiocarbon, pCO_2 varies from 278 to 354 µatm [51]. We do not consider isotopic fractionation between gaseous and dissolved $^{14}CO_2$, but our results can be compared with radiocarbon measurements reported as $\Delta^{14}C$, which is corrected for these effects.

A.2. Terrestrial biosphere model

In the simulations of Heinrich events the ocean is coupled to an atmospheric reservoir and to a model of the land biosphere [54], which consists of four compartments representing the ground vegetation plus leaves, wood, detritus and soils. All carbon reservoirs are considered as well-mixed. For the present-day experiments (HPD) we adopt the reservoir sizes and turnover times given by Siegenthaler and Oeschger [54]. In the glacial experiments (HGS), the reservoir sizes are reduced by 29% for the atmosphere and by 22% for each biosphere compartment, which is equivalent to a pCO_2 drop by 80 µatm and to a total decrease of terrestrial biomass by 500 Pg carbon [55], respectively. The Siegenthaler–Oeschger model accounts for isotopic fractionation between atmosphere and biosphere. However, following Stocker and Wright [47], here the fractionation factors are all set to 1 because all model results are directly interpreted as $\Delta^{14}C$ (see also above). The model biosphere dampens the atmospheric $\Delta^{14}C$ increase during the freshwater perturbations by up to 16‰.

References

[1] S.-J. Kim, G. Flato, G. Boer, A coupled climate model simulation of the Last Glacial Maximum: Part 2. Approach to equilibrium, Clim. Dyn. 20 (2003) 635–661.

[2] C.D. Hewitt, A.J. Broccoli, J.F.B. Mitchell, R. Stouffer, A coupled model study of the last glacial maximum: was part of the North Atlantic relatively warm? Geophys. Res. Lett. 28 (2001) 1571–1574.

[3] C. Wunsch, Determining paleoceanographic circulations, with emphasis on the Last Glacial Maximum, Quat. Sci. Rev. 22 (2003) 371–385.

[4] J.-M. Campin, T. Fichefet, J.-C. Duplessy, Problems with using radiocarbon to infer ocean ventilation rates for past and present climates, Earth Planet. Sci. Lett. 165 (1999) 17–24.

[5] A.M.E. Winguth, D. Archer, J.-C. Duplessy, E. Maier-Reimer, U. Mikolajewicz, Sensitivity of paleonutrient tracer distributions and deep-sea circulations to glacial boundary conditions, Paleoceanography 14 (1999) 304–323.

[6] K.J. Meissner, A. Schmittner, A.J. Weaver, J.F. Adkins, Ventilation of the North Atlantic Ocean during the Last Glacial Maximum: a comparison between simulated and observed radiocarbon ages, Paleoceanography 18 (2003) 1023.

[7] A. Schmittner, Southern Ocean sea ice and radiocarbon ages of glacial bottom waters, Earth Planet. Sci. Lett. 213 (2003) 53–62.

[8] M. Schulz, A. Paul, Sensitivity of the ocean-atmosphere carbon cycle to ice-covered and ice-free conditions in the Nordic Seas during the Last Glacial Maximum, Palaeogeogr. Palaeoclimatol. Palaeoecol. 207 (2004) 127–141.

[9] S.-I. Shin, Z. Liu, B.L. Otto-Bliesner, J.E. Kutzbach, S.J. Vavrus, Southern Ocean sea-ice control of the glacial North Atlantic thermohaline circulation, Geophys. Res. Lett. 30 (2003) 1096.
[10] E. Bard, M. Arnold, B. Hamelin, N. Tisnerat-Laborde, G. Cabioch, Radiocarbon calibration by means of mass spectrometric $^{230}Th/^{234}U$ and ^{14}C ages of corals: an updated database including samples from Barbados, Mururoa and Tahiti, Radiocarbon 40 (1998) 1085–1092.
[11] H. Kitagawa, J. van der Plicht, Atmospheric radiocarbon calibration to 45,000 yr B.P.: Late Glacial fluctuations and cosmogenic isotope production, Science 279 (1998) 1187–1190.
[12] E. Maier-Reimer, U. Mikolajewicz, K. Hasselmann, Mean circulation of the Hamburg LSG OGCM and its sensitivity to the thermohaline surface forcing, J. Phys. Oceanogr. 23 (1993) 731–757.
[13] C. Schäfer-Neth, A. Paul, Circulation of the glacial Atlantic: a synthesis of global and regional modeling, in: P. Schäfer, W. Ritzrau, M. Schlüter, J. Thiede (Eds.), The Northern North Atlantic: A Changing Environment, Springer, Berlin, 2001, pp. 446–462.
[14] M. Prange, G. Lohmann, A. Paul, Influence of vertical mixing on the thermohaline hysteresis: analyses of an OGCM, J. Phys. Oceanogr. 33 (2003) 1707–1721.
[15] CLIMAP Project Members, Seasonal reconstructions of the Earth's surface at the Last Glacial Maximum, Geological Society of America Map Chart Series, MC-36, Geological Society of America, Boulder, Colorado, 1981, pp. 1–18.
[16] G. Lohmann, S. Lorenz, On the hydrological cycle under paleoclimatic conditions as derived from AGCM simulations, J. Geophys. Res. 105 (2000) 17417–17436.
[17] M. Sarnthein, R. Gersonde, S. Niebler, U. Pflaumann, R. Spielhagen, J. Thiede, G. Wefer, M. Weinelt, Overview of Glacial Atlantic Ocean Mapping (GLAMAP 2000), Paleoceanography 18 (2003) 1030.
[18] A. Paul, C. Schäfer-Neth, Modeling the water masses of the Atlantic Ocean at the Last Glacial Maximum, Paleoceanography 18 (2003) 1058.
[19] M. Prange, G. Lohmann, V. Romanova, M. Butzin, Modelling tempo-spatial signatures of Heinrich Events: influence of the climatic background state, Quat. Sci. Rev. 23 (2004) 521–527.
[20] J.R. Toggweiler, K. Dixon, K. Bryan, Simulations in a coarse-resolution world ocean model, 1. Steady state prebomb distributions, J. Geophys. Res. 94 (1989) 8217–8242.
[21] M.E. Fiadeiro, Three-dimensional modeling of tracers in the deep Pacific Ocean, II. Radiocarbon and the circulation, J. Mar. Res. 40 (1982) 537–550.
[22] F. Joos, J.C. Orr, U. Siegenthaler, Ocean carbon transport in a box diffusion versus a general circulation model, J. Geophys. Res. 102 (1997) 12367–12388.
[23] R.M. Key, A. Kozyr, C.L. Sabine, K. Lee, R. Wanninkhof, J.L. Bullister, R.A. Feely, F.J. Millero, C. Mordy, T.-H. Peng, A global ocean carbon climatology: results from GLODAP, Glob. Biogeochem. Cycles 18 (2004) GB4031.
[24] M. Stuiver, T.F. Braziunas, Modeling atmospheric ^{14}C influences and ^{14}C ages of marine samples to 10,000 BC, Radiocarbon 35 (1993) 137–189.
[25] V. Romanova, M. Prange, G. Lohmann, Stability of the glacial thermohaline circulation and its dependence on the background hydrological cycle, Clim. Dyn. 22 (2004) 527–538.
[26] W.S. Broecker, et al., Accelerator mass spectrometry radiocarbon measurements on marine carbonate samples from deep sea cores and sediment traps, Radiocarbon 30 (1988) 261–295.
[27] N.J. Shackleton, J.-C. Duplessy, M. Arnold, P. Maurice, M.A. Hall, J. Cartlidge, Radiocarbon age of glacial Pacific deep water, Nature 355 (1988) 708–711.
[28] J.-C. Duplessy, M. Arnold, E. Bard, A. Juillet-Leclerc, N. Kallel, L. Labeyrie, AMS ^{14}C study of transient events and of the ventilation rate of the Pacific intermediate water during the last deglaciation, Radiocarbon 31 (1989) 493–502.
[29] W.S. Broecker, T.-H. Peng, S. Trumbore, G. Bonani, W. Wolfi, The distribution of radiocarbon in the glacial ocean, Glob. Biogeochem. Cycles 4 (1990) 103–117.
[30] A. van Geen, R.G. Fairbanks, P. Dartnell, M. McCann, J.V. Gardner, M. Kashgarian, Ventilation changes in the northeast Pacific during the last deglaciation, Paleoceanography 11 (1996) 519–528.
[31] J.F. Adkins, H. Cheng, E.A. Boyle, E.R.M. Druffel, R.L. Edwards, Deep-sea coral evidence for rapid change in ventilation of the deep North Atlantic 15,400 years ago, Science 280 (1998) 725–728.
[32] A. Mangini, M. Lomitschka, R. Eichstädter, N. Frank, S. Vogler, G. Bonani, I. Hajdas, J. Pätzold, Coral provides way to age deep water, Nature 392 (1998) 347–348.
[33] E.L. Sikes, C.R. Samson, T.P. Guilderson, W.R. Howard, Old radiocarbon ages in the southwest Pacific Ocean during the last glacial period and deglaciation, Nature 405 (2000) 555–559.
[34] S.J. Goldstein, D.W. Lea, S. Chakraborty, M. Kashgarian, M.T. Murrell, Uranium-series and radiocarbon geochronology of deep-sea corals: implications for Southern Ocean ventilation rates and the oceanic carbon cycle, Earth Planet. Sci. Lett. 193 (2001) 167–182.
[35] W.S. Broecker, Constraints on the glacial operation of the Atlantic Ocean's conveyor circulation, Isr. J. Chem. 42 (2002) 1–14.
[36] L.D. Keigwin, Late Pleistocene–Holocene paleoceanography and ventilation of the Gulf of California, J. Oceanogr. 58 (2002) 421–432.
[37] L.D. Keigwin, M.A. Schlegel, Ocean ventilation and sedimentation since the glacial maximum at 3 km in the western North Atlantic, Geochem. Geophys. Geosyst. 3 (2002) 1034.
[38] W.S. Broecker, E. Clark, I. Hajdas, G. Bonani, Glacial ventilation rates for the deep Pacific Ocean, Paleoceanography 19 (2004) PA2002.
[39] W.S. Broecker, S. Barker, E. Clark, I. Hajdas, G. Bonani, L. Stott, Ventilation of the glacial deep Pacific Ocean, Science 306 (2004) 1169–1172.

[40] J.F. Adkins, K. McIntyre, D.P. Schrag, The salinity, temperature and $\delta^{18}O$ content of the glacial deep ocean, Science 280 (2002) 1769–1773.

[41] S.R. Hemming, Massive late Pleistocene detritus layers of the North Atlantic and their global climate imprint, Rev. Geophys. 42 (2004) RG1005.

[42] J. Masarik, J. Beer, Simulation of particle fluxes and cosmogenic nuclide production in the Earth's atmosphere, J. Geophys. Res. 104 (1999) 12099–13012.

[43] R. Muscheler, J. Beer, G. Wagner, C. Laj, C. Kissel, G.M. Raisbeck, F. Yiou, P.W. Kubik, Changes in the carbon cycle during the last deglaciation as indicated by the comparison of ^{10}Be and ^{14}C records, Earth Planet. Sci. Lett. 6973 (2004) 1–16.

[44] E. Bard, M. Arnold, J. Mangerud, M. Paterne, L. Labeyrie, J. Duprat, M.-A. Mélières, E. Sønstegard, J.-C. Duplessy, The North Atlantic atmosphere–sea surface ^{14}C gradient during the Younger Dryas climatic event, Earth Planet. Sci. Lett. 126 (1994) 275–287.

[45] U. Mikolajewicz, A meltwater induced collapse of the conveyor belt thermohaline circulation and its influence on the distribution of $\Delta^{14}C$ and $\delta^{18}O$ in the oceans, Report No. 189, Max-Planck-Institut für Meteorologie, Hamburg (1996) 25 pp.

[46] K.A. Hughen, J.T. Overpeck, S.C. Lehman, M. Kashgarian, J. Southon, L.C. Peterson, R. Alley, D.M. Sigman, Deglacial changes in ocean circulation from an extended radiocarbon calibration, Nature 391 (1998) 65–68.

[47] T.F. Stocker, D.G. Wright, Rapid changes in ocean circulation and atmospheric radiocarbon, Paleoceanography 11 (1996) 773–796.

[48] O. Marchal, T.F. Stocker, R. Muscheler, Atmospheric radiocarbon during the Younger Dryas: production, ventilation, or both? Earth Planet. Sci. Lett. 185 (2001) 383–395.

[49] G. Delaygue, T.F. Stocker, F. Joos, G.-K. Plattner, Simulation of atmospheric radiocarbon during abrupt oceanic circulation changes: trying to reconcile models and reconstructions, Quat. Sci. Rev. 22 (2003) 1647–1658.

[50] K. Hughen, S. Lehman, J. Southon, J. Overpeck, O. Marchal, C. Herring, J. Turnbull, ^{14}C activity and global carbon cycle changes over the past 50,000 years, Science 203 (2004) 202–207.

[51] I.G. Enting, T.M.L. Wigley, M. Heimann, Future emissions and concentrations of carbon dioxide: key ocean/atmosphere/land analyses, electronic edition 2001, CSIRO Division of Atmospheric Research Technical Paper, vol. 31, CSIRO Atmospheric Research, Viktoria, Australia, 1994, 118 pp.

[52] R.F. Weiss, Carbon dioxide in water and seawater: the solubility of a non-ideal gas, Mar. Chem. 2 (1974) 203–215.

[53] R. Wanninkhof, Relationship between wind speed and gas exchange over the ocean, J. Geophys. Res. 97 (1992) 7373–7382.

[54] U. Siegenthaler, H. Oeschger, Biospheric CO_2 emissions during the past 200 years reconstructed by deconvolution of ice core data, Tellus 39B (1987) 140–154.

[55] I.C. Prentice, G.D. Farquhar, M.J.R. Fasham, M.L. Goulden, M. Heimann, V.J. Jaramillo, H.S. Kheshgi, C. Le Quéré, R.J. Scholes, D.W.R. Wallace, The carbon cycle and atmospheric carbon dioxide, in: J.T. Houghton, Y. Ding, D.J. Griggs, M. Noguer, P.J. van der Linden, X. Dai, K. Maskell, C.A. Johnson (Eds.), Climate Change 2001: The Scientific Basis. Contribution of Working Group I to the Third Assessment Report of the Intergovernmental Panel on Climate Change, Cambridge University Press, Cambridge, 2001, pp. 183–238.

[56] P.U. Clark, N.G. Pisias, T.F. Stocker, A.J. Weaver, The role of the thermohaline circulation in abrupt climate change, Nature 415 (2002) 863–869.